Hindawi Publishing Corporation
Journal of Nanomaterials
Volume 2016, Article ID 1207907, 9 pages
http://dx.doi.org/10.1155/2016/1207907

Research Article

Nanostructured Fe_2O_3 Based Composites Prepared through Arc Plasma Method as Anode Materials in the Lithium-Ion Battery

Minpeng Liang,[1] Jianxin Zou,[1,2] Xiaoqin Zeng,[1,2] and Wenjiang Ding[1,2]

[1]*National Engineering Research Center of Light Alloy Net Forming & State Key Laboratory of Metal Matrix Composites, Shanghai Jiao Tong University, Shanghai 200240, China*
[2]*Shanghai Engineering Research Center of Magnesium Materials and Applications & School of Materials Science and Engineering, Shanghai Jiao Tong University, Shanghai 200240, China*

Correspondence should be addressed to Jianxin Zou; zoujx@sjtu.edu.cn

Received 18 October 2016; Accepted 24 November 2016

Academic Editor: Xuezhang Xiao

In the present work, a method combining arc plasma evaporation of a metal followed by oxidation in air was developed to produce nanosized metal oxide based composites in large scale. As an example, Fe_2O_3 based nanocomposites were prepared through such a method. With increasing the oxidation temperature, α-Fe_2O_3 content in the composites increases, while γ-Fe_2O_3 and residual α-Fe contents decrease. As anode materials for lithium batteries, the electrochemical properties of nanosized Fe_2O_3 composites were tested. It was found that the anode materials changed to tiny crystallites and then followed by grain growth during the galvanostatic charge/discharge cycles. A capacity rising was observed for the composites obtained at 400°C and 450°C, which was more prominent with increasing the oxidation temperature. Among these composites, the one obtained at 450°C showed the best performance: a specific capacity of 507.6 mAh/g remained after 150 cycles at a current density of 200 mA/g, much higher than that of the commercial nano-Fe_2O_3 powder (~180 mAh/g after 30 cycles).

1. Introduction

Nowadays, along with the rapid growing consumption of energy, efficient and advanced electrochemical energy conversion and storage devices become more and more important in our daily life. Lithium-ion battery, as a kind of rechargeable battery with many outstanding features, is essential for the development of modern products, such as portable electronic devices and electric vehicles. Current commercial lithium-ion batteries (LIBs) use graphite as anode material, which has a theoretical capacity of only 372 mAh/g. Such a capacity is insufficient for many applications. To improve the storage capacity, alternative anode materials are highly desired [1–6].

In the past decades, enormous efforts have been taken to develop new anode materials other than graphite, such as carbon based materials, Si based materials, and metal oxides. Iron oxide, as one of the transition metal oxides, has attracted much attention due to its high theoretical capacity up to 1007 mAh/g, nontoxicity, and good corrosion resistance in electrolyte [7–9]. However, despite these appealing features, iron oxides often suffer from poor capacity retention and cycling stability due to their intrinsical hysteresis, drastic volume change (~96%), and low electrical conductivity during the charge/discharge process. To solve these problems, iron oxide based composites with different nanostructures and additives were developed and tested in Li-ion batteries [3]. In recent years, it is observed that iron oxide composites containing either carbon based or other metal oxides based additives have outstanding charge/discharge performances. For instance, Cho et al. [10] synthesized nanostructured Fe_2O_3-carbon nanofibers by combining the Kirkendall effect with the electrospinning method that exhibited enhanced structural stability during long-term cycling. Following an unusual route, Zhu and coworkers [11] prepared a kind of reduced graphene oxide/Fe_2O_3 composite, which showed good cycling performance and rate capability as anode material in the lithium-ion battery. Similar iron oxide composites

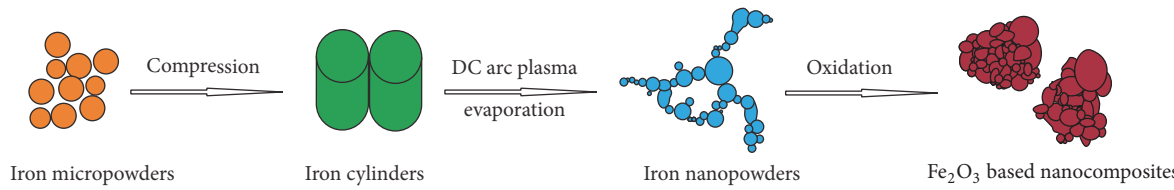

Figure 1: Schematic illustration of the preparation of Fe_2O_3 based nanocomposites.

containing carbon based materials had also been reported, for example, carbon-coated α-Fe_2O_3 [12], carbon-encapsulated Fe_3O_4 [13], graphene-wrapped Fe_3O_4 [14], and α-Fe_2O_3 nanoparticle-loaded carbon nanofiber composites [9]. The metal oxide based Fe_2O_3 composites have also been used as high-performance anode materials including Fe_2O_3/Co_3O_4 [15], Fe_2O_3/β-MnO_2 [8], Fe_2O_3/SnO_2 [16], and Fe_2O_3/TiO_2 [17–19]. Although Fe_2O_3 itself as anode material has some intrinsic disadvantages relative to the composites of Fe_2O_3, pure Fe_2O_3 having special nanostructures, such as hollow spheres [20], nanofibers [21], nanoflakes [22], nanorods [23–26], and mesoporous structures [7, 27–29], show outstanding performances. These nanostructures help to improve the thermodynamics and kinetics properties of Fe_2O_3 based materials as anode of LIBs. Nevertheless, it is still a challenge for material scientists to produce such qualified anodic materials in large scale and low cost. Therefore, it is necessary to develop efficient approaches for preparing Fe oxides based anode materials.

In contrast to conventional method to obtain Fe_2O_3 through the precursors of FeOOH or $Fe(OH)_3$ (FeOOH/$Fe(OH)_3$ $\rightarrow$ Fe_2O_3 + H_2O), the present work focused on a new processing route through direct oxidation of the nanosized iron powders (Fe + O_2 $\rightarrow$ Fe_2O_3). Such a method can also be employed to produce other kinds of metal/alloy oxides in large scale. Another goal of this study is to understand the structural changes and electrochemical properties of Fe_2O_3 as the anode material of LIBs during charge/discharge processes.

2. Materials and Methods

2.1. Materials. Reduced iron powders and sodium alginate were purchased from Aladdin. Button-type cell (2032), lithium foil, separator, and the electrolyte (1 M LiPF6 dissolved in a mixture solvent of ethylene carbonate (EC), dimethyl carbonate (DMC), and diethyl carbonate (DEC) in a volume ratio of 1 : 1 : 1) were purchased from Shenzhen Kejing Co. (China).

2.2. Preparation of Fe_2O_3 Based Nanocomposites. The procedure of producing Fe_2O_3 based nanocomposites is schematically shown in Figure 1.

2.2.1. The Preparation of Iron Nanopowders via DC Arc Plasma Evaporation Method [30, 31]. The starting materials were reduced iron powders with a particle size of about 150 μm. These powders were compressed at room temperature to form cylinders with 10 mm in diameter and 15 mm in height by a uniaxial compressor under a pressure of 12 MPa for 2 minutes. Then the bulk specimens were put into the reaction chamber under a mixture of 55 kPa Ar and 35 kPa H_2 gas after the chamber was evacuated to below 5×10^{-2} Pa. The current was set as 150 A for the arc evaporation process. After the evaporation, the reaction chamber was cooled down to room temperature followed by the addition of more air until the pressure went up to 100 kPa. Then the nanosized iron powders were passivated for 6 h to form a thin oxide layer on the nanoparticles and prevent spontaneous burning in air.

2.2.2. The Oxidation of Iron Nanopowders. The nanosized Fe_2O_3 based composites were prepared by heating the iron nanopowders in a Muffle furnace at 250°C, 350°C, 400°C, and 450°C in air for 2 h. These composite samples are named as sample Fe_2O_3-250, sample Fe_2O_3-350, sample Fe_2O_3-400, and sample Fe_2O_3-450 according to their oxidation temperatures.

2.3. Characterizations. X-ray diffraction (XRD) measurements were performed on an apparatus (Rigaku, D/max 2550 VL/PCX) equipped with a Cu-Kα radiation source in the 2θ range from 10° to 90°. A field-emission transmission electron microscope (TEM, JEM 2100F) was used to acquire the microstructures and the details about crystal lattice of different phases in samples.

2.4. Cell Preparation and Electrochemical Measurements. The electrochemical properties of the Fe_2O_3 based composites were studied by assembling a button-type cell (2032) in an argon-filled glove box with both water and oxygen concentration less than 1.7 ppm. The working electrodes were prepared by mixing the active materials, acetylene black and binder (sodium alginate) [32], in a weight ratio of 8 : 1 : 1, which were then coated on copper foils followed by drying under vacuum at 60°C for 6 hours to remove the solvent (water). The density of active material was around 1.3–1.6 g/cm^2. The lithium foil was used as both counter electrode and reference electrode, and the separator was Celgard 2400. The electrolyte was 1 M $LiPF_6$ dissolved in a mixture solvent of ethylene carbonate (EC), dimethyl carbonate (DMC), and diethyl carbonate (DEC) in a volume ratio of 1 : 1 : 1. The properties of cyclic voltammetry (CV) and galvanostatic charge/discharge cycling were tested. The CV curves were acquired using an electrochemical workstation (CHI 660E) at the scanning rate of 0.1 mV/s with a potential range of 0.01–3 V. The galvanostatic charge/discharge measurements were carried out using a lithium battery cycler (LAND CT-2001A) at the current density of 200 mA/g with a cut-off potential

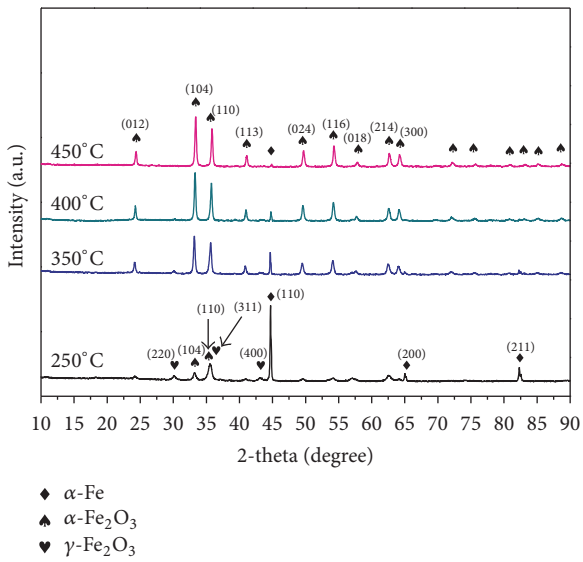

FIGURE 2: XRD patterns of Fe_2O_3 based nanocomposites obtained at different temperatures.

window of 0.01–3 V. All these electrochemical measurements were conducted at ambient temperature.

3. Results and Discussions

3.1. Structural and Morphological Analyses of Fe_2O_3 Based Nanocomposites. The XRD patterns of Fe_2O_3 based nanocomposites are shown in Figure 2. At 250°C, the composites contain α-Fe, α-Fe_2O_3, and γ-Fe_2O_3. The strongest peak belongs to α-Fe, indicating that the main phase in this composite is iron. With increasing the temperature, the intensity of α-Fe and γ-Fe_2O_3 peaks decreases while intensity of peaks corresponding to α-Fe_2O_3 increases, indicating an increasing content of α-Fe_2O_3 phase in the composite with the increasing temperature. When temperature reaches 450°C, α-Fe and γ-Fe_2O_3 almost disappear, as displayed in Figure 2. The PDF cards used above are JCPDS number 33-0664 for α-Fe_2O_3 (hematite), JCPDS number 39-1346 for γ-Fe_2O_3 (maghemite), and JCPDS number 65-4899 for α-Fe.

The typical microstructure of the iron nanopowders prepared by DC Arc plasma method is shown in Figure 3(a). It can be seen that the iron nanoparticles with their size ranging from 20 nm to 300 nm form "nanochains." After heating in air, the iron nanopowders were oxidized and aggregated together. The morphology has changed somehow greatly due to the oxidation induced structure and volume changes. This can be confirmed by TEM images of Figures 3(b), 3(d), 3(f), and 3(h), which show the powders oxidized at 250°C, 350°C, 400°C, and 450°C, respectively. As seen in the high resolution TEM images of different samples, such as sample Fe_2O_3-250 (Figure 3(c)), sample Fe_2O_3-350 (Figure 3(e)), sample Fe_2O_3-400 (Figure 3(g)), and sample Fe_2O_3-450 (Figure 3(i)), the interplanar spacings of 0.27 nm and 0.23 nm correspond well to the (104) and (006) planes of α-Fe_2O_3, respectively.

3.2. Electrochemical Analyses. Figure 4(b) displays the first five cyclic voltammetry (CV) curves of sample Fe_2O_3-350. In the first cathodic scan, a sharp reduction peak appears at ~0.51 V, which can be attributed to the reduction of Fe_2O_3 to Fe, the formation of a solid electrolyte interphase film (SEI), and some irreversible reactions [10, 22]. For the anodic process, one broad peak is observed at ~1.64 V, which can be ascribed to the oxidation of Fe to Fe^{2+} and then to Fe^{3+} [33–35]. The reduction peaks of the later cycles shift to higher voltage at about 0.94 V, while the oxidation peaks do not change their positions and shapes. However, a sloped plateau exists at the right of the peak in the second reduction process, and the same situation also appears on other samples except the sample Fe_2O_3-450, as shown in Figure 4. Moreover, the sloped plateau disappears in the subsequent cycles, inferring a direct correlation with the irreversible structural changes of γ-Fe_2O_3. The structural changes of α-Fe_2O_3 and γ-Fe_2O_3 are particularly noteworthy since there is only one distinct peak observed during these cathodic/anodic scans. The appearance of the single peak can be attributed to the fact that there are continuous structural changes between α-Fe (cubic), α-Fe_2O_3 (rhombohedral), and γ-Fe_2O_3 (cubic) phases. It shows that no distinct boundary exists between α-Fe (cubic), γ-Fe_2O_3 (cubic or part of tetragonal), and α-Fe_2O_3 (rhombohedral) phases aligned from inside to outside of the Fe_2O_3 based composites. Indeed, during the first three cycles, in order to adjust the expansion/compression during lithiation/delithiation, some reversible or irreversible structure changes must occur on the Fe_2O_3 based composites. After the third cycle, only one peak is observed in the cathodic/anodic scans, suggesting that a one-step redox reaction is caused by a stable structural change of the Fe_2O_3 based composites.

To understand the one-step redox reaction in detail, XRD measurements were carried out for the sample Fe_2O_3-350 which stopped at 0.01 V and 3 V during the 3rd cycle, as depicted in Figure 5(a). Surprisingly, the XRD patterns at 3 V show identified peaks from α-Fe and several unnoticeable broad peaks from γ-Fe_2O_3, suggesting that the active material has changed to tiny crystallites. To further study the reaction mechanism, XRD analysis is carried out on the sample charged at 3 V for the 25th cycle (Figure 5(a)), which reveals complementary information about the status of the anode material. Comparing the curve 25-3 V and the curve 3-0.01 V, it can be found that they have some common peaks, which can be attributed to the formation of some irreversible products, such as Li_2O and $Li_xFe_2O_3$ [27]. On the other hand, the curve 25-3 V contains some unique peaks which can be ascribed to the phase of γ-Fe_2O_3. Although both of the curves, 3-0.01 V and 25-3 V, contain the same peaks from γ-Fe_2O_3 phase, there are inconspicuous peaks at 30.1° and 43.2° in the curve 3-3 V. There are also some peaks from several byproducts generated during irreversible reactions which are quite close to 30.1° and 43.2°. Moreover, the differences between the curves 3-3 V and 25-3 V, that is, more diffraction peaks and their higher intensity, indicate a grain growth of γ-Fe_2O_3 and some phases after charging/discharging cycles. It can be observed from Figure 4(e) that there is only one distinct peak during cathodic/anodic scans at the 25th cycle, inferring that the main active material is γ-Fe_2O_3 for the 25th cycle.

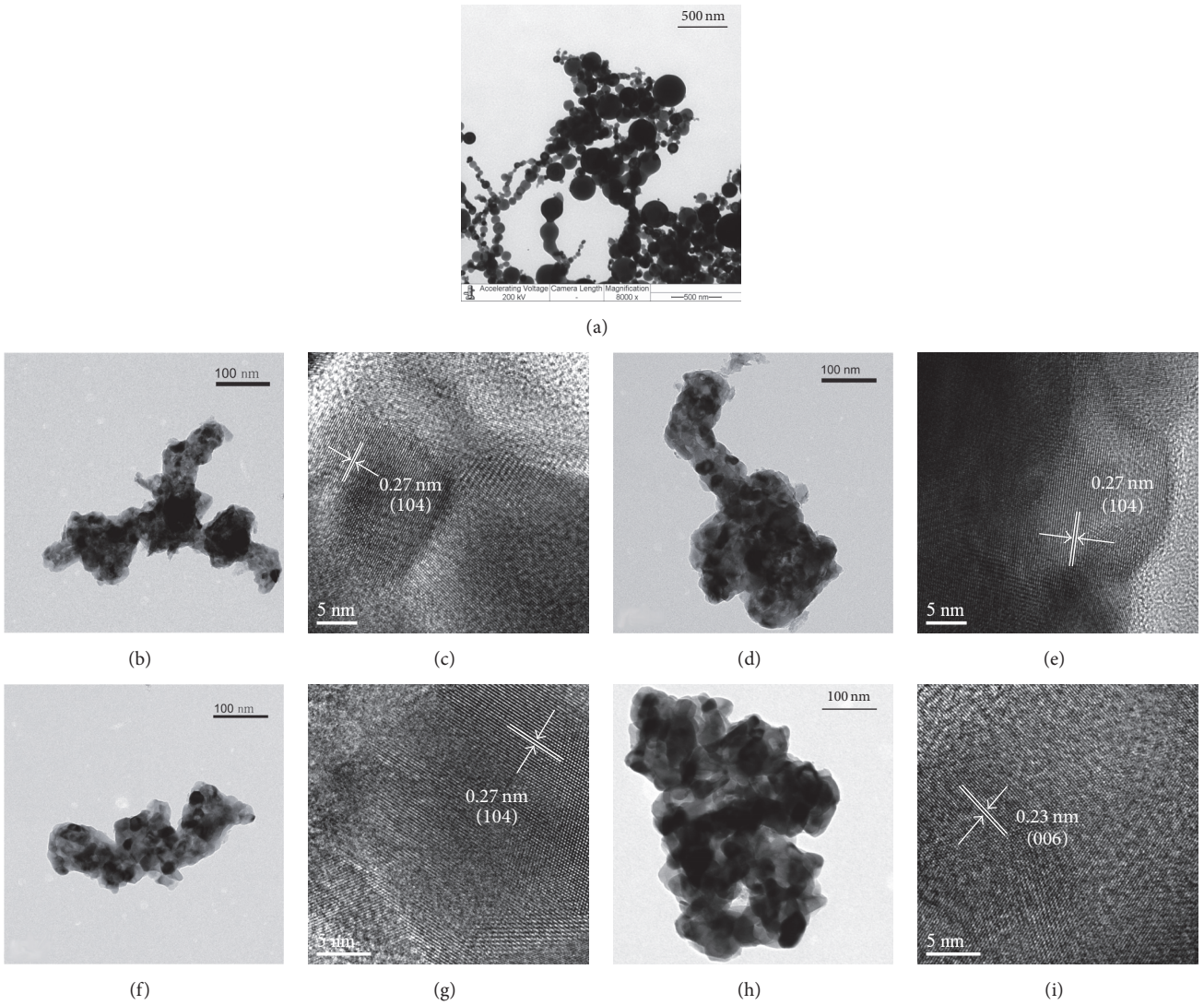

FIGURE 3: TEM images showing nanoparticles in iron nanopowder (a), samples Fe_2O_3—250 (b), Fe_2O_3-350 (d), Fe_2O_3-400 (f), and Fe_2O_3-450 (h) and their corresponding HRTEM images of samples: (c) Fe_2O_3-250, (e) Fe_2O_3-350, (g) Fe_2O_3-400, and (i) Fe_2O_3-450.

Figure 6(a) shows the cycling performance of Fe_2O_3 based nanocomposites at different oxidation temperatures (i.e., 250°C, 350°C, 400°C, and 450°C). As depicted in Figure 6(a), in terms of specific capacity and the stability of charging/discharging curves, the sample Fe_2O_3-350 shows a superior performance as compared to other composites during the first 74 cycles, but for the last 76 cycles, the sample Fe_2O_3-450 shows the best performance, with a reversible specific capacity of 507.6 mAh/g after 150 cycles. Although the sample Fe_2O_3-350 in general exhibits a higher specific capacity than the sample Fe_2O_3-250, its specific capacity undergoes a severe loss after 150 cycles, with 51.4% capacity retention for the sample Fe_2O_3-350 and 59.3% capacity retention for the sample Fe_2O_3-250 as compared to the 2nd cycle. The cycling performances of all of the simples are much better than the commercial nano-Fe_2O_3 powder which has a capacity of about 180 mAh/g that remained after only 30 cycles tested by Liu et al. [25] at a lower current density (100 mA/g). These results indicate that a higher Fe_2O_3 contents in the composite may lead to a higher initial specific capacity but lower cycling stability. This can be attributed to the large volume changes in Fe_2O_3 during lithium insertion/extraction process. Such a volume change causes a pulverization of electrodes and thereby leads to a poor cycling performance. The results clearly show that the degree of oxidation for a metal is crucial for its performance as the anode material of LIBs. On a closer examination of Figure 6(a), an interesting phenomenon can be observed for the sample Fe_2O_3-450 that the specific capacity drops drastically for the first 25 cycles with a noticeable fluctuation from the 10th to 25th cycle, and then the capacity increases constantly from the 25th cycle. Similar capacity rising phenomenon also exists for the sample Fe_2O_3-400, as shown in Figure 6(a). The discharge specific capacity of the sample Fe_2O_3-400 is increased from 383 mAh/g at the 25th cycle to 431 mAh/g at the 150th cycle. At the same time, the specific capacity of the sample

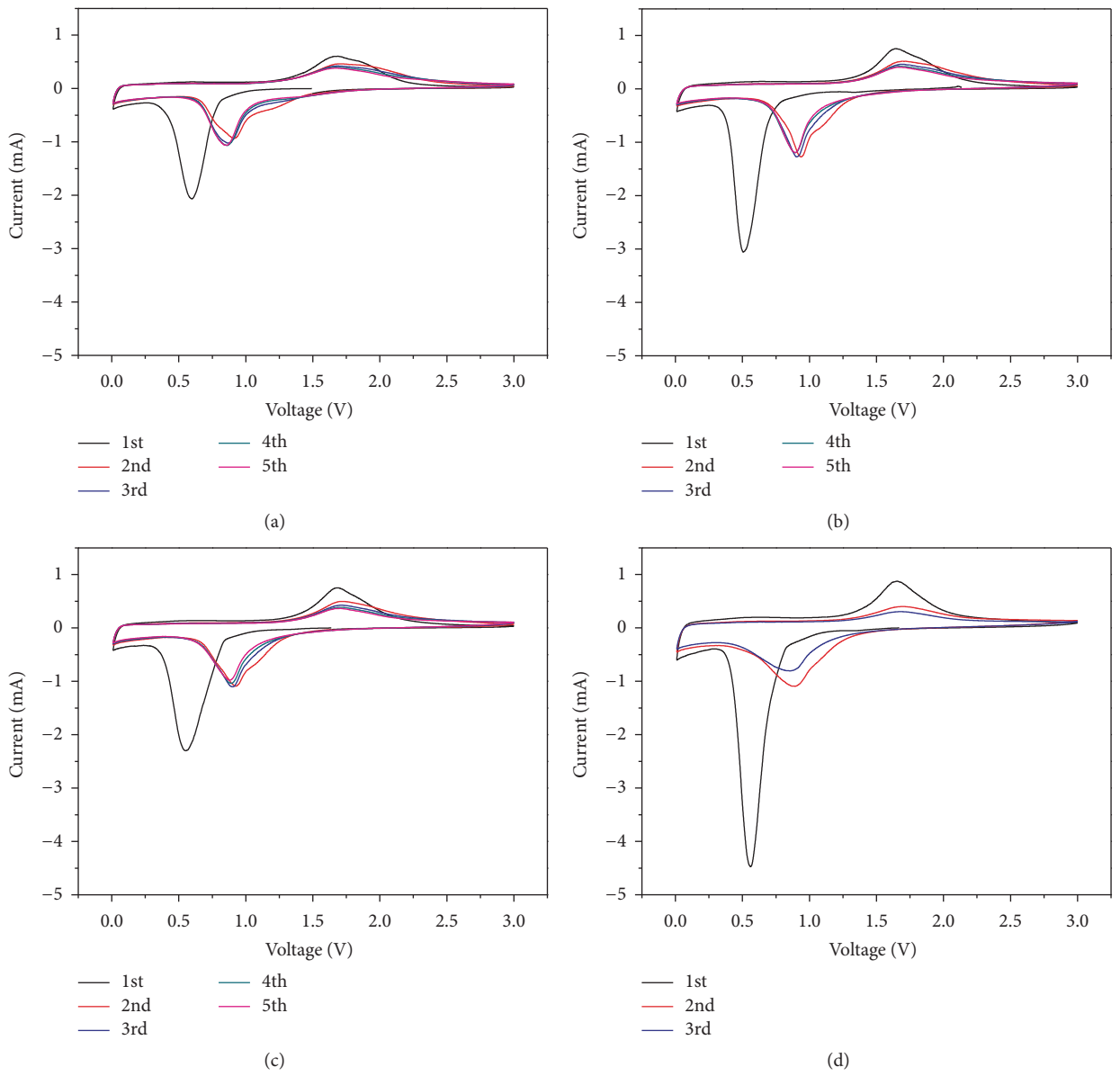

Figure 4: CV curves at a scan rate of 0.1 mV/s of samples Fe_2O_3-250 (a), Fe_2O_3-350 (b), Fe_2O_3-400 (c), and Fe_2O_3-450 (d) in a voltage range of 0.01–3 V (versus Li^+/Li).

Fe_2O_3-450 increases from 319.9 mAh/g at the 25th cycle to 507.6 mAh/g at the 150th cycle, which is much higher than that of sample Fe_2O_3-400. However, such a capacity rising phenomenon is not observed for sample Fe_2O_3-250 or sample Fe_2O_3-350. To further study this phenomenon, the voltage profiles of samples at their 1st, 2nd, 3rd, 25th, and 150th cycles are displayed in Figures 6(b), 6(c), 6(d), and 6(e).

Figure 6(b) shows the voltage profiles of the sample Fe_2O_3-250, for which the first discharge curve displays a long and flat plateau at ~0.76 V, while for the second discharge process, the curve shows a slope line with an average plateau voltage of ~0.98 V. During the subsequent discharging process, the plateau is steeper and the plateau voltage monotonically decreases to ~0.88 V at the 150th cycle, which may be attributed to the gradual irreversible changes of Fe_2O_3 during repeated lithium insertion and extraction [29]. Except the width of the plateau and the magnitude of the specific capacity, there are no other dissimilarities for the 1st, 2nd, 3rd, and 25th voltage profiles of all composite samples (Figures 6(b), 6(c), 6(d), and 6(e)). However, it is worth noting that the voltage profiles of the sample Fe_2O_3-250, sample Fe_2O_3-350, sample Fe_2O_3-400, and sample Fe_2O_3-450 at 150th cycle are quite different. For the sample Fe_2O_3-250 and the sample Fe_2O_3-350, the discharge curves of the 25th cycle and the 150th cycle almost overlap in the voltage range of 3–1.5 V, while the curves of the 150th cycle of the sample Fe_2O_3-400 and the sample Fe_2O_3-450 are more flat than that of 25th cycle at the same voltage range. Furthermore, in the voltage range of 0.01–1 V, the charge curves of the 150th cycle of the sample Fe_2O_3-400 and the sample Fe_2O_3-450 are also more flat than

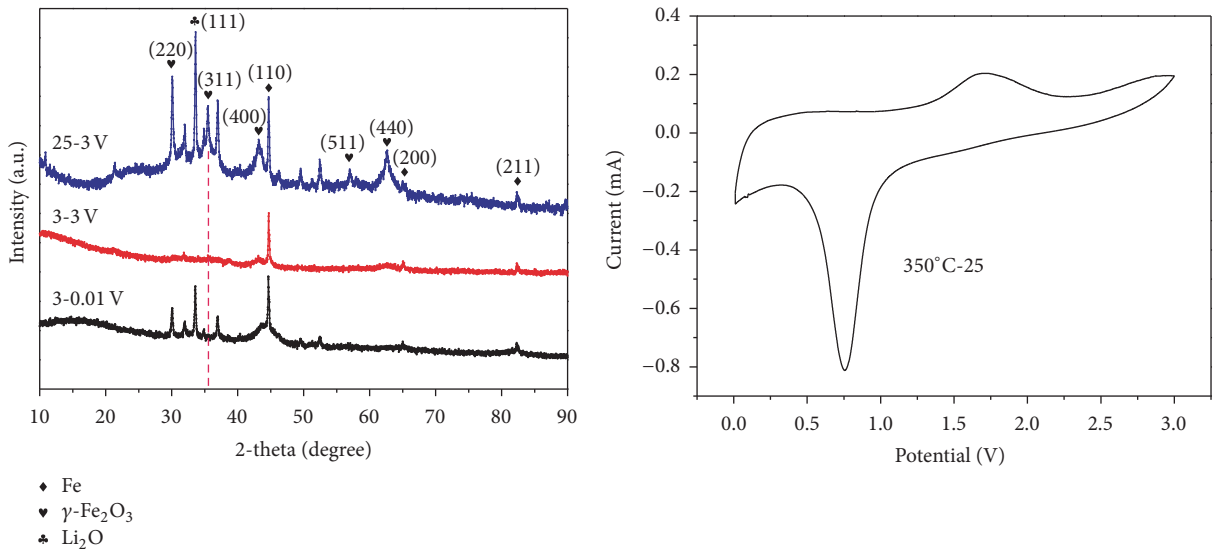

FIGURE 5: (a) XRD patterns of sample Fe_2O_3-350 during the 3rd and 25th galvanostatic charge/discharge cycles at 0.01 V and 3 V. (b) CV curve at a scan rate of 0.1 mV/s of sample Fe_2O_3-350 after 25 galvanostatic charge/discharge cycles.

that of the 25th cycle of the sample Fe_2O_3-250 and the sample Fe_2O_3-350, as shown in Figures 6(b), 6(c), 6(d), and 6(e). These results reveal that the processes occurring in the voltage range of 0.01–1 V and 1.5–3 V may partially contribute to the capacity rising phenomenon, similar to the results shown by Laruelle et al. [36]. As reported in the literature [37, 38], the choice of binder does not have any effect on the capacity rising phenomenon. However, such a phenomenon is not only seen in nanosized Fe_2O_3 composites, but also in other kinds of 3d transition metal oxides, which are also working through conversion reaction [3, 36], such as cobalt oxides [39] and manganese oxides [40, 41]. The phenomenon was usually attributed to the reversible growth of a gel-like layer catalyzed by 3d transition metals, as proposed by Laruelle et al. [36, 40], or the reversible interfacial reactions, as proposed by Jamnik et al. [37, 42]. The exact mechanism is not known yet, but it is possible that the active materials (i.e., Fe_xO_y, Fe +2 or +3) promote the capacity rising, no matter whether they accelerate the formation of gel-like layer or the reversible interfacial reactions. Indeed, the capacity rising starts from the 25th cycle, and the main active material is iron oxides. Moreover, comparing to the sample Fe_2O_3-450 with more obvious capacity rising, the sample Fe_2O_3-400 has a less amount of Fe_2O_3 (α and γ). Therefore, one can draw a conclusion that the more active materials the electrode contains, the more obvious the capacity rising phenomenon will be. Further work is undergoing to elucidate the exact mechanisms associated with such capacity rising involved in the present work.

4. Conclusions

For the first time, Fe_2O_3 based nanocomposites were prepared by oxidation of arc plasma evaporated nanoiron powders at different temperatures. Along with the increasing oxidation temperature, Fe_2O_3 based composites showed an increasing content of α-Fe_2O_3 and decreasing contents of α-Fe and γ-Fe_2O_3. When the composites were used as anode materials in lithium-ion battery, it was found that the active material (Fe_2O_3) showed a change into tiny crystallites at the first several galvanostatic charge/discharge cycles and then followed by crystallization and grain growth (γ-Fe_2O_3). A severe capacity loss occurred at the first several cycles for all the Fe_2O_3 based nanocomposites. However, a capacity rising was observed for the composites obtained at 400°C and 450°C, which was more obvious when the content of active material, Fe_2O_3, increased. For different Fe_2O_3 based nanocomposites as anode materials for lithium-ion batteries, the one obtained at 450°C exhibited the highest capacity of 507.6 mAh/g after 150 cycles, much higher than that of the commercial one (~180 mAh/g after 30 cycles). The method developed in this work can be also used to prepare other kinds of nanosized metal oxide powders as anode materials for lithium-ion batteries in large scale.

Competing Interests

The authors declare that they have no competing interests.

Acknowledgments

Professor Jianxin Zou would like to thank the support from the Science and Technology Committee of Shanghai under no. 14JC1491600. This work is partly supported by the National Natural Science Foundation of China (no. 51274140) and "Shuguang" Scholar Project (no. 16SG08) from Shanghai Education Commission.

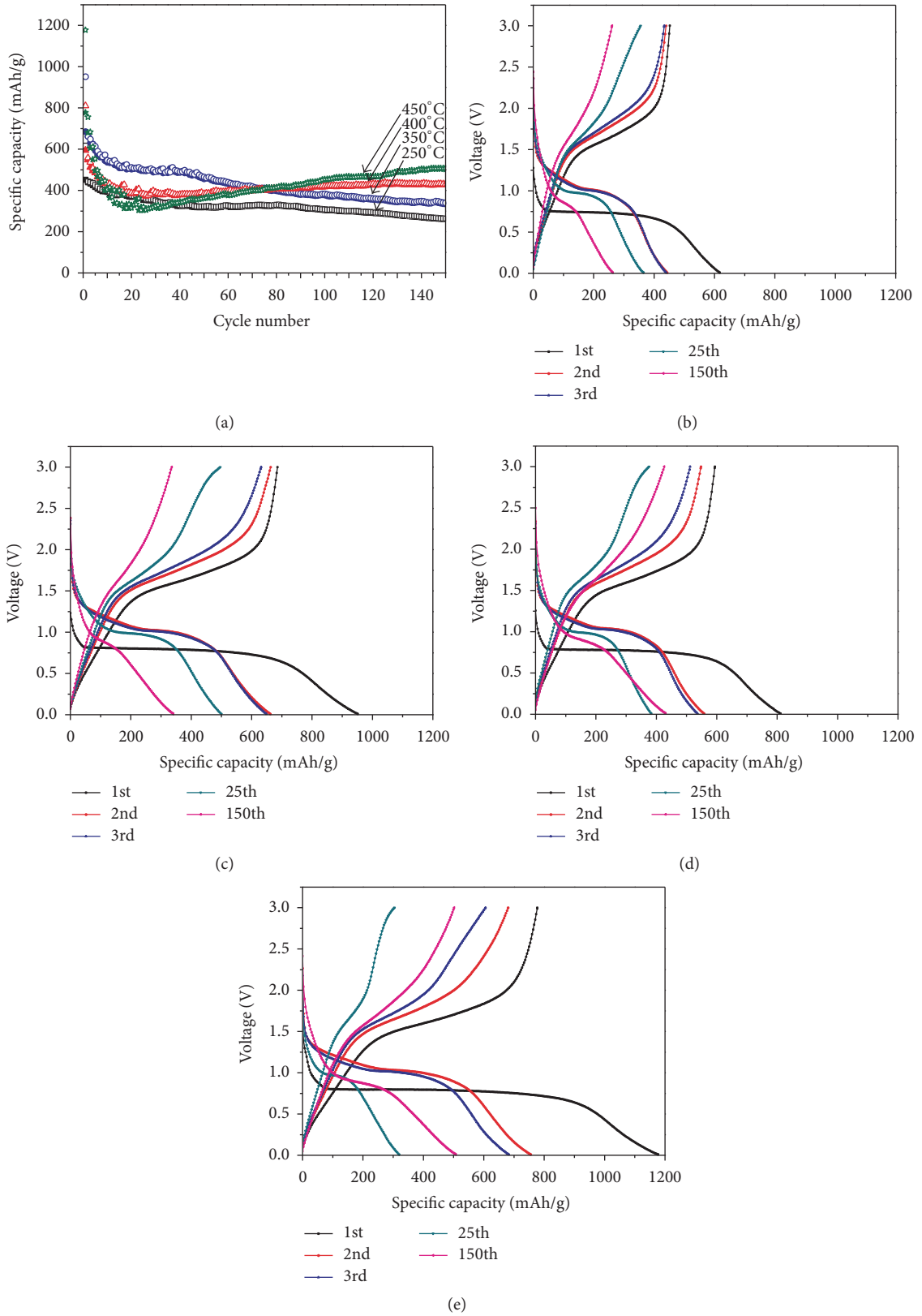

Figure 6: (a) Evolution of capacity with cycle numbers for Fe_2O_3 based nanocomposites measured at a current density of 200 mA/g and charge-discharge curves of samples Fe_2O_3-250 (b), Fe_2O_3-350 (c), Fe_2O_3-400 (d), and Fe_2O_3-450 (e).

References

[1] B. Scrosati, J. Hassoun, and Y.-K. Sun, "Lithium-ion batteries. A look into the future," *Energy and Environmental Science*, vol. 4, no. 9, pp. 3287–3295, 2011.

[2] N. Nitta and G. Yushin, "High-capacity anode materials for lithium-ion batteries: choice of elements and structures for active particles," *Particle and Particle Systems Characterization*, vol. 31, no. 3, pp. 317–336, 2014.

[3] H. B. Wu, J. S. Chen, H. H. Hng, and X. W. D. Lou, "Nanostructured metal oxide-based materials as advanced anodes for lithium-ion batteries," *Nanoscale*, vol. 4, no. 8, pp. 2526–2542, 2012.

[4] K. C. Klavetter, J. Pedro De Souza, A. Heller, and C. B. Mullins, "High tap density microparticles of selenium-doped germanium as a high efficiency, stable cycling lithium-ion battery anode material," *Journal of Materials Chemistry A*, vol. 3, no. 11, pp. 5829–5834, 2015.

[5] H. Jia, P. Gao, J. Yang, J. Wang, Y. Nuli, and Z. Yang, "Novel three-dimensional mesoporous silicon for high power lithium-ion battery anode material," *Advanced Energy Materials*, vol. 1, no. 6, pp. 1036–1039, 2011.

[6] C. Han, D. Yang, Y. Yang et al., "Hollow titanium dioxide spheres as anode material for lithium ion battery with largely improved rate stability and cycle performance by suppressing the formation of solid electrolyte interface layer," *Journal of Materials Chemistry A*, vol. 3, no. 25, pp. 13340–13349, 2015.

[7] H. Dong, Y. Xu, M. Ji, H. Zhang, Z. Zhao, and C. Zhao, "High performance of mesoporous γ-Fe_2O_3 nanoparticle/Ketjen Black composite as anode material for lithium ion batteries," *Electrochimica Acta*, vol. 151, pp. 118–125, 2015.

[8] X. Gu, L. Chen, Z. Ju, H. Xu, J. Yang, and Y. Qian, "Controlled growth of porous α-Fe_2O_3 branches on β-MnO_2 nanorods for excellent performance in lithium-ion batteries," *Advanced Functional Materials*, vol. 23, no. 32, pp. 4049–4056, 2013.

[9] L. Ji, O. Toprakci, M. Alcoutlabi et al., "α-Fe_2O_3 nanoparticle-loaded carbon nanofibers as stable and high-capacity anodes for rechargeable lithium-ion batteries," *ACS Applied Materials and Interfaces*, vol. 4, no. 5, pp. 2672–2679, 2012.

[10] J. S. Cho, Y. J. Hong, and Y. C. Kang, "Design and synthesis of bubble-nanorod-structured Fe_2O_3 carbon nanofibers as advanced anode material for Li-Ion batteries," *ACS Nano*, vol. 9, no. 4, pp. 4026–4035, 2015.

[11] X. Zhu, Y. Zhu, S. Murali, M. D. Stoller, and R. S. Ruoff, "Nanostructured reduced graphene oxide/Fe_2O_3 composite as a high-performance anode material for lithium ion batteries," *ACS Nano*, vol. 5, no. 4, pp. 3333–3338, 2011.

[12] X. Lv, J. Deng, J. Wang, J. Zhong, and X. Sun, "Carbon-coated α-Fe_2O_3 nanostructures for efficient anode of Li-ion battery," *Journal of Materials Chemistry A*, vol. 3, no. 9, pp. 5183–5188, 2015.

[13] C. He, S. Wu, N. Zhao, C. Shi, E. Liu, and J. Li, "Carbon-encapsulated Fe_3O_4 nanoparticles as a high-rate lithium ion battery anode material," *ACS Nano*, vol. 7, no. 5, pp. 4459–4469, 2013.

[14] G. Zhou, D.-W. Wang, F. Li et al., "Graphene-wrapped Fe_3O_4 anode material with improved reversible capacity and cyclic stability for lithium ion batteries," *Chemistry of Materials*, vol. 22, no. 18, pp. 5306–5313, 2010.

[15] Q. Q. Xiong, X. H. Xia, J. P. Tu et al., "Hierarchical Fe_2O_3@Co_3O_4 nanowire array anode for high-performance lithium-ion batteries," *Journal of Power Sources*, vol. 240, pp. 344–350, 2013.

[16] W. Zhou, C. Cheng, J. Liu et al., "Epitaxial growth of branched α-Fe_2O_3/SnO_2 nano-heterostructures with improved lithium-ion battery performance," *Advanced Functional Materials*, vol. 21, no. 13, pp. 2439–2445, 2011.

[17] Y. Fu, Q. Wei, X. Wang, H. Shu, X. Yang, and S. Sun, "Porous hollow α-Fe_2O_3@TiO_2 core–shell nanospheres for superior lithium/sodium storage capability," *Journal of Materials Chemistry A*, vol. 3, no. 26, pp. 13807–13818, 2015.

[18] X. Zhang, H. Chen, Y. Xie, and J. Guo, "Ultralong life lithium-ion battery anode with superior high-rate capability and excellent cyclic stability from mesoporous Fe_2O_3@TiO_2 core-shell nanorods," *Journal of Materials Chemistry A*, vol. 2, no. 11, pp. 3912–3918, 2014.

[19] L. Li, J. Zhang, and Q. Zhu, "A novel fractional crystallization route to porous TiO_2-Fe_2O_3 composites: large scale preparation and high performances as a photocatalyst and Li-ion battery anode," *Dalton Transactions*, vol. 45, no. 7, pp. 2888–2896, 2016.

[20] B. Wang, J. S. Chen, H. B. Wu, Z. Wang, and X. W. Lou, "Quasiemulsion-templated formation of α-Fe_2O_3 hollow spheres with enhanced lithium storage properties," *Journal of the American Chemical Society*, vol. 133, no. 43, pp. 17146–17148, 2011.

[21] S. Chaudhari and M. Srinivasan, "1D hollow α-Fe_2O_3 electrospun nanofibers as high performance anode material for lithium ion batteries," *Journal of Materials Chemistry*, vol. 22, no. 43, pp. 23049–23056, 2012.

[22] M. V. Reddy, T. Yu, C.-H. Sow et al., "α-Fe_2O_3 nanoflakes as an anode material for li-ion batteries," *Advanced Functional Materials*, vol. 17, no. 15, pp. 2792–2799, 2007.

[23] C. T. Cherian, J. Sundaramurthy, M. Kalaivani et al., "Electrospun α-Fe_2O_3 nanorods as a stable, high capacity anode material for Li-ion batteries," *Journal of Materials Chemistry*, vol. 22, no. 24, pp. 12198–12204, 2012.

[24] Y.-M. Lin, P. R. Abel, A. Heller, and C. B. Mullins, "α-Fe_2O_3 nanorods as anode material for lithium ion batteries," *The Journal of Physical Chemistry Letters*, vol. 2, no. 22, pp. 2885–2891, 2011.

[25] H. Liu, G. Wang, J. Park, J. Wang, H. Liu, and C. Zhang, "Electrochemical performance of α-Fe_2O_3 nanorods as anode material for lithium-ion cells," *Electrochimica Acta*, vol. 54, no. 6, pp. 1733–1736, 2009.

[26] X. Yao, C. Tang, G. Yuan, P. Cui, X. Xu, and Z. Liu, "Porous hematite (α-Fe_2O_3) nanorods as an anode material with enhanced rate capability in lithium-ion batteries," *Electrochemistry Communications*, vol. 13, no. 12, pp. 1439–1442, 2011.

[27] B. Sun, J. Horvat, H. S. Kim, W.-S. Kim, J. Ahn, and G. Wang, "Synthesis of mesoporous α-Fe_2O_3 nanostructures for highly sensitive gas sensors and high capacity anode materials in lithium ion batteries," *Journal of Physical Chemistry C*, vol. 114, no. 44, pp. 18753–18761, 2010.

[28] J. Wang, M. Gao, H. Pan et al., "Mesoporous Fe_2O_3 flakes of high aspect ratio encased within thin carbon skeleton for superior lithium-ion battery anodes," *Journal of Materials Chemistry A*, vol. 3, no. 27, pp. 14178–14187, 2015.

[29] Y. Xu, G. Jian, Y. Liu, Y. Zhu, M. R. Zachariah, and C. Wang, "Superior electrochemical performance and structure evolution of mesoporous Fe_2O_3 anodes for lithium-ion batteries," *Nano Energy*, vol. 3, pp. 26–35, 2014.

[30] H. Shao, T. Liu, Y. Wang, H. Xu, and X. Li, "Preparation of Mg-based hydrogen storage materials from metal nanoparticles," *Journal of Alloys and Compounds*, vol. 465, no. 1-2, pp. 527–533, 2008.

[31] Y. Sakka, H. Okuyama, T. Uchikoshi, and S. Ohno, "Synthesis and characterization of Fe and composite Fe-TiN nanoparticles by dc arc-plasma," *Journal of Alloys and Compounds*, vol. 346, no. 1-2, pp. 285–291, 2002.

[32] I. Kovalenko, B. Zdyrko, A. Magasinski et al., "A major constituent of brown algae for use in high-capacity Li-ion batteries," *Science*, vol. 334, no. 6052, pp. 75–79, 2011.

[33] X. Cui, Y. Zhu, F. Li et al., "Enhanced rate capability of a lithium ion battery anode based on liquid-solid-solution assembly of Fe_2O_3 on crumpled graphene," *RSC Advances*, vol. 6, no. 11, pp. 9007–9012, 2016.

[34] F. Zheng, M. He, Y. Yang, and Q. Chen, "Nano electrochemical reactors of Fe_2O_3 nanoparticles embedded in shells of nitrogen-doped hollow carbon spheres as high-performance anodes for lithium-ion batteries," *Nanoscale*, vol. 7, no. 8, pp. 3410–3417, 2015.

[35] J. Qiu, M. Li, Y. Zhao, Q. Kong, X. Li, and C. Li, "Scalable synthesis of nanometric α-Fe_2O_3 within interconnected carbon shells from pyrolytic alginate chelates for lithium storage," *RSC Adv.*, vol. 6, no. 10, pp. 7961–7969, 2016.

[36] S. Laruelle, S. Grugeon, P. Poizot, M. Dollé, L. Dupont, and J.-M. Tarascon, "On the origin of the extra electrochemical capacity displayed by MO/Li cells at low potential," *Journal of the Electrochemical Society*, vol. 149, no. 5, pp. A627–A634, 2002.

[37] J. Li, H. M. Dahn, L. J. Krause, D.-B. Le, and J. R. Dahn, "Impact of binder choice on the performance of α-Fe_2O_3 as a negative electrode," *Journal of the Electrochemical Society*, vol. 155, no. 11, pp. A812–A816, 2008.

[38] Y. Jiang, D. Zhang, Y. Li et al., "Amorphous Fe_2O_3 as a high-capacity, high-rate and long-life anode material for lithium ion batteries," *Nano Energy*, vol. 4, pp. 23–30, 2014.

[39] S. Grugeon, S. Laruelle, L. Dupont, and J.-M. Tarascon, "An update on the reactivity of nanoparticles Co-based compounds towards Li," *Solid State Sciences*, vol. 5, no. 6, pp. 895–904, 2003.

[40] J. Yue, X. Gu, L. Chen et al., "General synthesis of hollow MnO_2, Mn_3O_4 and MnO nanospheres as superior anode materials for lithium ion batteries," *Journal of Materials Chemistry A*, vol. 2, no. 41, pp. 17421–17426, 2014.

[41] Q. Hao, J. Wang, and C. Xu, "Facile preparation of Mn_3O_4 octahedra and their long-term cycle life as an anode material for Li-ion batteries," *Journal of Materials Chemistry A*, vol. 2, no. 1, pp. 87–93, 2014.

[42] J. Jamnik and J. Maier, "Nanocrystallinity effects in lithium battery materials: aspects of nano-ionics. Part IV," *Physical Chemistry Chemical Physics*, vol. 5, no. 23, pp. 5215–5220, 2003.